ACS Photonics

pubs.acs.org/journal/apchd5

Letter

Dynamic Control of Plasmonic Localization by Inverse Optimization of Spatial Phase Modulation

Doksoo Lee,[†] Shizhou Jiang,[†] Oluwaseyi Balogun, and Wei Chen*

Cite This: *ACS Photonics* 2022, 9, 351−359

Read Online

ACCESS | Metrics & More | Article Recommendations | Supporting Information

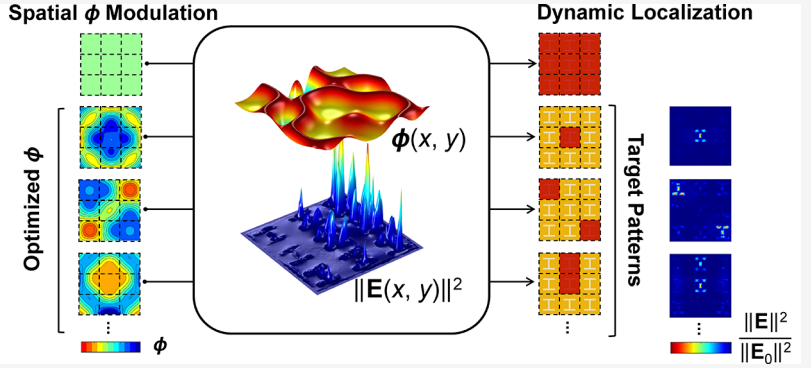

ABSTRACT: We present a systematic inverse design approach to achieve digitally addressable plasmonic metasurfaces. Beyond existing literature, we adopt a variety of input phase profiles to control the local optical field distribution on the metasurface. Our inverse design approach relies on three building blocks. First, we model the spatial phase distribution of the incident field using a linear superposition of harmonic functions to generate smooth and flexible phase distributions. Second, we propose a localization scheme to quantify the local optical field concentration on the metasurface. Third, Bayesian optimization is employed to learn the underlying nonlinear mapping and to reduce the number of numerical simulations needed to reach the target hotspot arrangements. The obtained computational designs can be implemented with a spatial light modulator to enable dynamic reconfiguration of diverse high-contrast localization patterns on a metasurface without mechanical scanning. The advanced dynamic addressability could fuel relevant applications beyond proof-of-concept demonstrations.

KEYWORDS: *active light control, plasmonic metasurface, spatial phase modulation, Bayesian optimization*

Optical metasurfaces are artificially engineered ultrathin structures that can support exotic light propagation using subwavelength elements that lead to enhanced electromagnetic fields at the nanoscale.[1−3] Metasurfaces have been intensely studied as a promising platform to facilitate practical nanophotonics applications because such planar arrays mitigate high resistive loss and low fabricability that bulk metamaterials usually suffer from.[1,4] Within the last two decades, advancements in design and nanomanufacturing of optical metasurfaces have led to broad applications including perfect absorption,[5] super resolution imaging,[6] and beam steering,[7−9] to name a few. As a branch of optical metamaterials, plasmonic metasurfaces build on metallic nanostructures. Their optical responses are dominated by the local surface plasmons (LSP), namely, the coupling of photons and electrons at the interface between plasmonic structures and dielectrics.[10] LSP underpins advance nano-optical sensing applications (Figure S1 in Supporting Information), where local perturbations to the electromagnetic field around nanoscale optical elements are detected at the far-field detector, thus facilitating super-resolution imaging beyond the fundamental optical diffraction limit.[11−16]

Active light control of plasmonic metasurfaces is a promising approach to enable high-throughput nanoscale optical imaging using far-field optical components. The technique relies on two building blocks, namely, plasmonic nanostructures that funnel propagating light into localized evanescent electromagnetic waves on the sample surface and spatial control of the locally enhanced electromagnetic wave field based on the phase of the input propagating light.[17] These building blocks facilitate nanoscale imaging without sample scanning, thus, eliminating motion artifacts and slow image acquisition due to mechanical actuators and scanning systems. Classical optical detection or

Received: July 12, 2021
Published: December 28, 2021

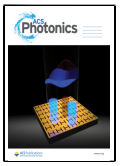

https://doi.org/10.1021/acsphotonics.1c01043
ACS Photonics 2022, 9, 351−359

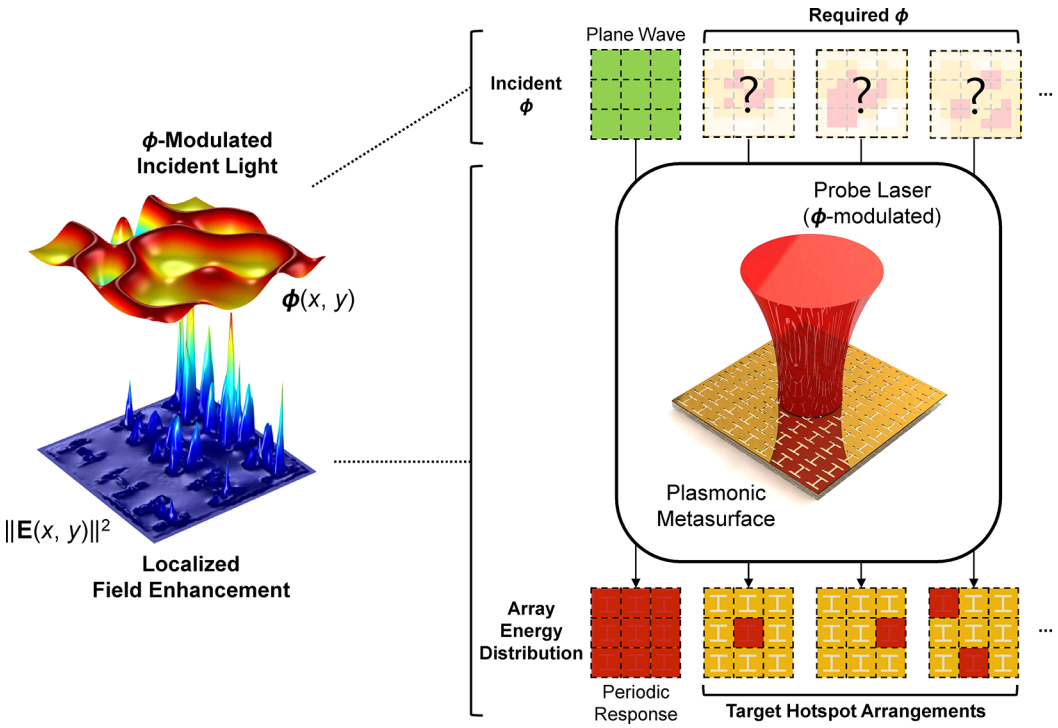

Figure 1. Conceptual illustration of SPM-driven dynamic light control. Plane wave excitation over a periodic plasmonic metasurface leads to periodic responses over the metasurface array. SPM breaks the periodicity of incident phase, which builds potential to induce arbitrary localization patterns. Hence, SPM forms an inverse problem on incident phase. This works aims to identify phase profiles that give rise to user-defined localization patterns on a stationary metasurface.

imaging approaches have limited spatial resolution due to far-field diffraction. Plasmonic nanoantennas provide a means to extend the spatial resolution to the nanoscale through the excitation of LSPs. However, conventional approaches for optical readout of nanoantenna arrays rely on static illumination profiles that address either a single nanoantenna in a sparse array or a collection of nanoantennas in a dense array. If one wants to address specific nanoantennas in an array, it is unavoidable to resort to mechanical adjustment of either the illumination and collection optics or the sample. One approach to address the limited flexibility and efficiency is to actively control the incident wavefield.

To advance active control of light confinement on plasmonic metasurfaces, existing works have reported various modulation methods of the incident wavefield, including polarization, phase, amplitude, and others. Sentenac et al.[18] implemented a phase conjugation method to calculate both the amplitude and the phase of the incident field needed to focus the light source at a specific position on a silicon-encapsulated 2D subwavelength grating. Through adaptive optimization, Aeschlimann et al.[19] experimentally showed that modulating the polarization of a femtosecond laser pulse can facilitate the realization of arbitrary light localization on a three-dimer system with rotational symmetry. Singh et al.[20] also demonstrated in experiments the rotation of hotspots at the ends of a nanoantenna by changing the polarization of the incident wavefield. Buijs et al.[21] optimized the amplitude and phase of the incident wavefield and numerically demonstrated programmable near-field light localizations in a 4 × 4 dipole array with a spatial resolution down to $\lambda/16$. However, the polarization modulation has limited control of plasmonic localization. Furthermore, the simultaneous modulation of amplitude and phase of the incident wavefield may be difficult to realize in practice.

Spatial phase modulation (SPM) offers an effective route to dynamically tailor light confinement on plasmonic metasurfaces (Figure 1). This idea relies on aperiodic phase lag of incident light source and a near-field interaction between discrete subwavelength scatters.[22] Compared to the approaches introduced above, SPM stands out in terms of its great ability for dynamic control of plasmonic localization and experimental feasibility to be easily reproduced by commercial spatial light modulators (SLMs). As an early work, Kao et al.[23] experimentally demonstrated coherent light control on a metasurface comprised of asymmetric split-ring resonators. Harmonically modulated phase profiles were used to realize the translation of a hotspot in a "digital" precision. Contrary to the global continuous profiles in the work just mentioned, a local discrete phase representation was also proposed for applications to super-resolution scattering.[24] In the discrete phase space, the authors employed a random combinatoric search to realize shifting of plasmonic hotspots. Gjonaj et al.[25] utilized surface plasmonic polaritons to actively control constructive interference at will. The results show intensity enhancement of the target spot 20× stronger compared to the surrounding with a simple device setup and an optimization loop for the discrete phase map. But the use of surface plasmonic polaritons only allows narrow localization areas (∼2 μm) and makes the system sensitive to the surrounding dielectrics, even for the single localization pattern presented.

Previous reports in the literature building on SPM have relied on brute-force trial-and-error approaches and greedy searches within narrow phase design spaces to identify the incident phase profiles for spatial control of plasmonic fields. Limited exploration of the design space leads to weak spatial

https://doi.org/10.1021/acsphotonics.1c01043
ACS Photonics 2022, 9, 351−359

confinement that allows unwanted off-target localization. Additionally, each work demonstrated only a single pattern on a predetermined meta-atom geometry. The state-of-the-art functionality may suffice as a proof-of-concept of SPM-driven light control, but not for the practical use. Optical detection systems (Figure S1 in the Supporting Information), for example, will suffer from the weak contrast of energy distributions since the sensing quality largely depends on the signal-to-noise ratio. The monotonous patterns limit the data acquisition capacity of the optical systems to only the cases where a single meta-atom at a predefined position is allowed. The phase-driven light control has potential to overcome such issues if the contrast and a diversity of hotspot arrangements can be enhanced. We believe that the technological leap demands intelligent exploration of large design freedom in metamaterial systems, in particular that of the space of incident phase modulation, beyond the narrow landscape addressed by the previous works.

Producing diverse user-defined localization patterns by SPM forms a demanding inverse problem on the incident phase (Figure 1). From a design optimization viewpoint, the main challenges we intend to address are as follows:

- High dimensional (high-D) physical quantities of interest (inputs of phase distributions and outputs of electric fields) render the optimization formulation ambiguous and the design search intractable (Figure 1).
- Full-wave analysis under aperiodic input phases is more resource-intensive than unit cell simulations under periodic boundary conditions. Modern optimization methods[26−31] usually involve a few hundred iterations to reach optimum. Exhaustive approaches[32−35] that are widely implemented in the parametric design of electromagnetic (EM) systems are computationally prohibitive for the full-wave analysis under aperiodic input phase.
- Gradient-based topology optimization approaches[26,27] are difficult to implement because a closed-form design sensitivity with respect to the incident phase is not available. Even in other EM design problems, where geometry design is of interest and such a sensitivity can be derived,[28] the search is prone to being trapped in local optima and suffers from poor convergence involved with material interpolation schemes of plasmonic structures.[36]

To overcome the aforementioned challenges, we propose a systematic inverse design approach on incident phase. The design objective is to identify a set of incident phase profiles that generate "on-demand" diverse localization patterns over a stationary plasmonic metasurface. The novel design approach builds on three main pillars: harmonic phase representation, localization measure, and Bayesian optimization (BO). Regarding input phase, we propose an extension of the phase representation employed in Kao et al.[23] Our representation generates smooth and flexible phase profiles that can be easily tuned by a small set of design parameters. We will show that with the proposed design representation, the optimization results can achieve diverse hotspot arrangements. To encode high-D output fields involving high-Q plasmonic resonance, we devise a localization measure that maps the electric field of the whole metasurface to a response matrix. The response matrix reduces the dimensionality of raw field profiles with preserving collective field intensity on individual meta-atoms, which facilitates inverse optimization with respect to a target energy distribution. BO[29−31,37] is implemented to efficiently identify global optimum without design sensitivity. BO can significantly cut down the costly EM solver calls with respect to the whole array compared to using evolutionary algorithms. In addition, a derivative-free search of BO is robust to local optima that prevail in EM design space.

We validate the proposed design method via numerical simulations of the electromagnetic field distributions in a two-dimensional array of gold I-beam metasurfaces,[14] in which diverse localization patterns are realized. Such user-defined responses in a digital precision can hardly be achieved by a conventional greedy search due to the strongly coupled optical responses between neighboring meta-atoms. Our approach could systematically identify multiple on-demand patterns to produce various arrangements of hotspots, contrary to existing works that only support a single pattern. The proposed inverse design achieves stronger spatial selectivity and diversity of hotspot distributions. It is noteworthy that the diverse localization patterns can switch from one to another rapidly. The shift rate is comparable to that of piezoelectric control, while our method allows larger flexibility (switching patterns) with less impact on samples (no mechanical adjustment of stage). The proposed phase design approach is applicable to general nanoantenna baselines[6,38−46] without modification, in addition to the I-beam baseline,[6] in particular, for augmenting metasurfaces with digital addressability. Potential applications include sensors,[47] optical tweezers,[48] and optical data storage,[49] to name a few.

PHASE REPRESENTATION

We propose a phase representation based on the harmonics superposition that will be realized in practice on the surface of an SLM. An optical imaging system illustrated in Figure S1 will be used to project the SLM phase profile onto the metasurface that is positioned at the focal plane of the imaging microscope objective. The field distribution on the SLM is imaged onto the metasurface with a demagnification factor of M. The imaging system has an object plane on the surface of the SLM. An intermediate image plane is formed at the back-focal plane of the microscope objective, where the spatial Fourier transform of the optical field at the object plane is formed. The inverse Fourier transform of the field at back-focal plane is formed on the focal plane of the microscope. Specifying a phase space for SPM is crucial for achieving on-demand hotspot arrangements. Phase lags that spatially vary across meta-atoms enable a geometrically periodic metasurface to output aperiodic localization. A phase representation can take any arbitrary formulation as long as it meets the requirements on resolution and smoothness imposed by a SLM. We propose the continuous phase representation as the following:

$$\phi(x,y) = \sum_{j=1}^{n_h} \varphi_j \Phi_j(x,y) = \sum_{j=1}^{n_h} \varphi_j \cos\left(\frac{\pi}{j\Lambda} Mx + \alpha_j\right)\cos\left(\frac{\pi}{j\Lambda} My + \beta_j\right)$$
$$\text{and } 0 \le \varphi_j \le \pi;\ \ 0 \le \alpha_j \le 2\pi;\ \ 0 \le \beta_j \le 2\pi \quad (1)$$

where ϕ is the spatial phase lag function; n_h is order of the expansion; Φ_j is the j-th harmonic basis; φ_j denotes the amplitude of harmonic j; α_j and β_j determine a translational shift of harmonic j along the x- and y-direction, respectively; Λ is the periodicity of a meta-atom. The core distinction from the previous works[23] is that we consider superposition of different harmonics which are allowed for translational shifts along the

https://doi.org/10.1021/acsphotonics.1c01043
ACS Photonics 2022, 9, 351−359

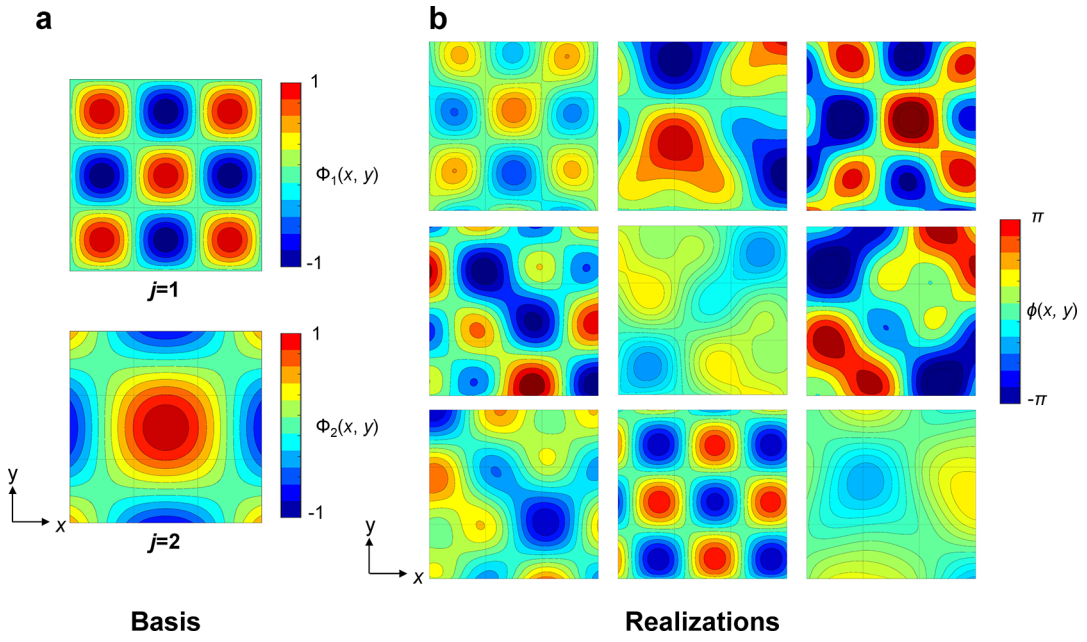

Figure 2. 2-D contour plots of the proposed incident phase representation on the SLM plane. The size of all the images shown here is $3\Lambda/M = 132$ μm. A particular distribution is fully specified by six design variables $\mathbf{X} = [\varphi_1, \alpha_1, \beta_1, \varphi_2, \alpha_2, \beta_2]^T$. Black grid lines denote borders between magnified meta-atoms. (a) Two basis functions of the representation. The period of the first-order term is set as $2\Lambda/M = (4/3)\lambda/M = 88$ μm. (b) Nine realizations generated from the proposed representation. The proposed representation produces smooth and flexible incident phase distributions by varying only six phase parameters that tune amplitude and shift of each harmonic.

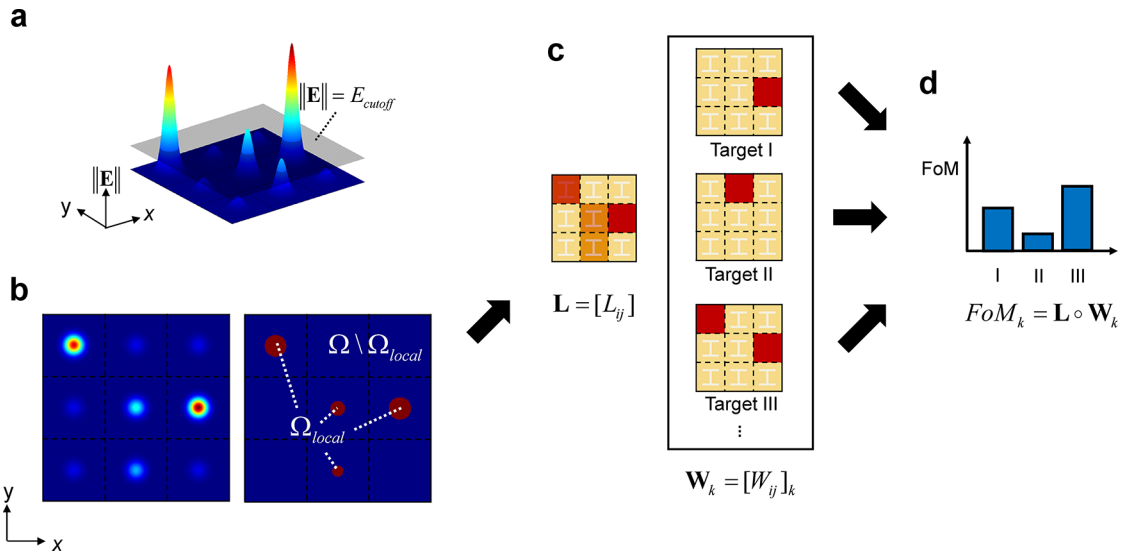

Figure 3. Proposed field processing scheme. (a) A virtual electric field profile $\mathbf{E}(x, y)$ with plasmonic resonances. A constant threshold E_{cutoff} is introduced to demarcate the user-defined localization domain from the whole analysis domain in a meta-atom. (b) Top view of the virtual field processing. Within a meta-atom indexed as (i, j), only the local intensity above the threshold E_{cutoff} contributes to L_{ij}. (c) A localization matrix $\mathbf{L}$ and weighting matrix $\mathbf{W}$. We convert the full-array field $\mathbf{E}$ to a response matrix $\mathbf{L} = [L_{ij}]$. $\mathbf{L}$ is scored based on a target hotspot arrangement. Each particular pattern involves $\mathbf{W}_k$, where k is the index of a target pattern. (d) The FoM to be maximized by optimization. Given a target $\mathbf{W}_k$, the FoM is computed by elementwise matrix multiplication ($\circ$). In this case, the given $\mathbf{E}$ field will get the highest score when Target III is the on-demand pattern of optimization.

two axes. An individual harmonic is specified by three design variables $[\varphi_j, \alpha_j, \beta_j]^T$. For $n_h = 2$ in our work, a phase profile is defined by six design variables $\mathbf{X} = [\varphi_1, \alpha_1, \beta_1, \varphi_2, \alpha_2, \beta_2]^T$. Details on the choice of $n_h = 2$ can be found in Section 2 of the Supporting Information. Figure 2 illustrates the bases and several realizations of our representation. It shows a large flexibility of the proposed representation in generating arbitrary distributions that can be fully specified by the small set of design variables. Some existing works[24,25] adopt local phase representations that assign a parameter to each meta-atom. The number of phase parameters would increase as the array size does. In contrast, our phase space is represented by global phase parameters: the number of design variables remains unchanged. Compared to the local representations that rely on independent discrete parameters, our approach offers smooth and spatially correlated distributions that have

https://doi.org/10.1021/acsphotonics.1c01043
ACS Photonics 2022, 9, 351−359

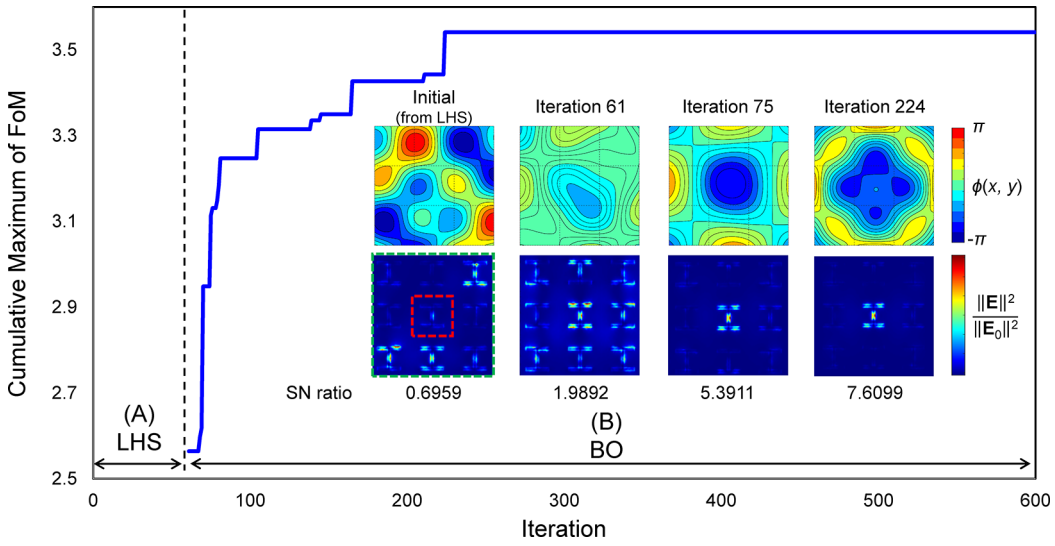

Figure 4. Optimization process for the center focus pattern. The optimization history consists of two stages: (A) sixty initial space-filling observations by Latin-hypercube sampling (LHS) and (B) sequential search guided by the acquisition function of Bayesian optimization. The observation labeled as "Initial" is one of the 60 LHS observations. The snapshots at a few selected iterations show the evolution of the input phase profiles (top row) and the corresponding energy distributions (bottom row). The signal-to-noise (SN) ratio of each pattern is computed as the energy density ratio between the target meta-atom (red) and off-target region (green), namely, SN = $(\int_{\Omega_{\text{target}}} \|\mathbf{E}(x, y)\|^2 \, d\Omega / \int_{\Omega_{\text{target}}} d\Omega)/(\int_{\Omega_{\text{off-target}}} \|\mathbf{E}(x, y)\|^2 \, d\Omega / \int_{\Omega_{\text{off-target}}} d\Omega)$. The field enhancement near the center meta-atom becomes intensified as the optimization proceeds, while unwanted off-target localization is noticeably suppressed.

physical interpretability. The electric field at SLM is given by incorporating the proposed phase modulation, eq 1, into the x-polarized incident wave as follows:

$$E_x = E_0 \exp\{i\phi(x, y)\} \tag{2}$$

where E_x is the x-component of the electric field; E_0 is the amplitude of the incident field. The field is incident to the metasurface through the imaging system shown in Figure S1, with diffraction included. To account for diffraction, we limit the allowable wavenumbers of the optical field at the focal plane of the microscope objective of the imaging system to smaller than the cutoff value of NA·k_0, where NA ≤ 1 is the numerical aperture of the objective and k_0 is the free-space wavevector.

LOCALIZATION MEASURE

We also devise a localization measure as a field processing scheme to combat the high dimensionality of plasmonic fields on the metasurface plane. It is challenging for design optimization to directly deal with raw plasmonic fields, since they often involve high-Q resonances in subwavelength scales (Figure 3a). Additionally, it could be desirable to collectively interpret plasmonic responses in a meta-atom unit, rather than analyzing details of local fields within meta-atoms. We propose the following integral-based measure:

$$L_{ij} = \frac{\int_{\Omega_{\text{local}}} \|\boldsymbol{E}(x, y)\| \, d\Omega}{\int_{\Omega} \|\boldsymbol{E}(x, y)\| \, d\Omega} \quad \text{where } \Omega_{\text{local}} = \{(x, y) | \|\boldsymbol{E}(x, y)\| \geq E_{\text{cutoff}}\} \tag{3}$$

where $\boldsymbol{E}(x, y)$ is the electric field on the metasurface plane, Ω is the planar measuring domain located right above the top face of a meta-atom, Ω_{local} is a subdomain of Ω, where field intensity exceeds the threshold, and L_{ij} is the localization measure of a meta-atom. The primary idea is to introduce a constant threshold E_{cutoff} that commonly applies to all field distributions of interest (Figure 3a) and to compute the ratio of the field intensity integrated over the localized domain Ω_{local} and the whole analysis domain Ω. Based on this definition, the localization measure is bounded between 0 and 1. Depending on the threshold value, a field distribution is mapped to a response matrix where each element corresponds to different spatial locations of a 2D array. Based on our numerical experiment, E_{cutoff} is set as $E_{\text{cutoff}} = 2E_0$. Given a single meta-atom, our field processing method maps norm of a field profile $\|\boldsymbol{E}\|$ into an $N \times N$ response matrix $L(\mathbf{X})$ when an $N \times N$ metasurface array is the system of interest (Figure 3c). This processing scheme enables us to quantify localization levels across meta-atoms. Additionally, we can directly use the compact response matrix as design objective for the subsequent inverse optimization in which we manipulate incident phase to attain a target localization. Note that evaluation of the same response matrix differs based on a target hotspot arrangement (Figure 3c,d).

We formulate the inverse phase optimization problem as

$$\begin{aligned} &\underset{\mathbf{X}=\{\varphi_j, \alpha_j, \beta_j\}}{\text{argmax:}} \; F(L(\mathbf{X})) = W \circ L = \sum_i^N \sum_j^N w_{ij} L_{ij} \\ &\text{subject to: } \varphi_j \in [0, \pi], \; \{\alpha_j, \beta_j\} \in [0, 2\pi] \end{aligned} \tag{4}$$

where L_{ij} is the localization measure from eq 3; N is the number of meta-atoms along either the x- or the y-axis; $L(\mathbf{X})$ is the localization matrix comprising localization measures of individual unit cells; w_{ij} is an element of the weighting matrix W determined by a target pattern; $\circ$ is the elementwise matrix multiplication operator. The localization level of individual meta-atoms is stored in $L(\mathbf{X})$ (Figure 3c). A weighted sum of the components $W \circ L$, given a desired localization pattern, can be used for evaluating how close an arbitrary field profile is to the target. Using the center focus scenario as an example (Figure 4), we set $W = [-1\ -1\ -1; -1\ 8\ -1; -1\ -1\ -1]$: w_{22}

https://doi.org/10.1021/acsphotonics.1c01043
ACS Photonics 2022, 9, 351−359

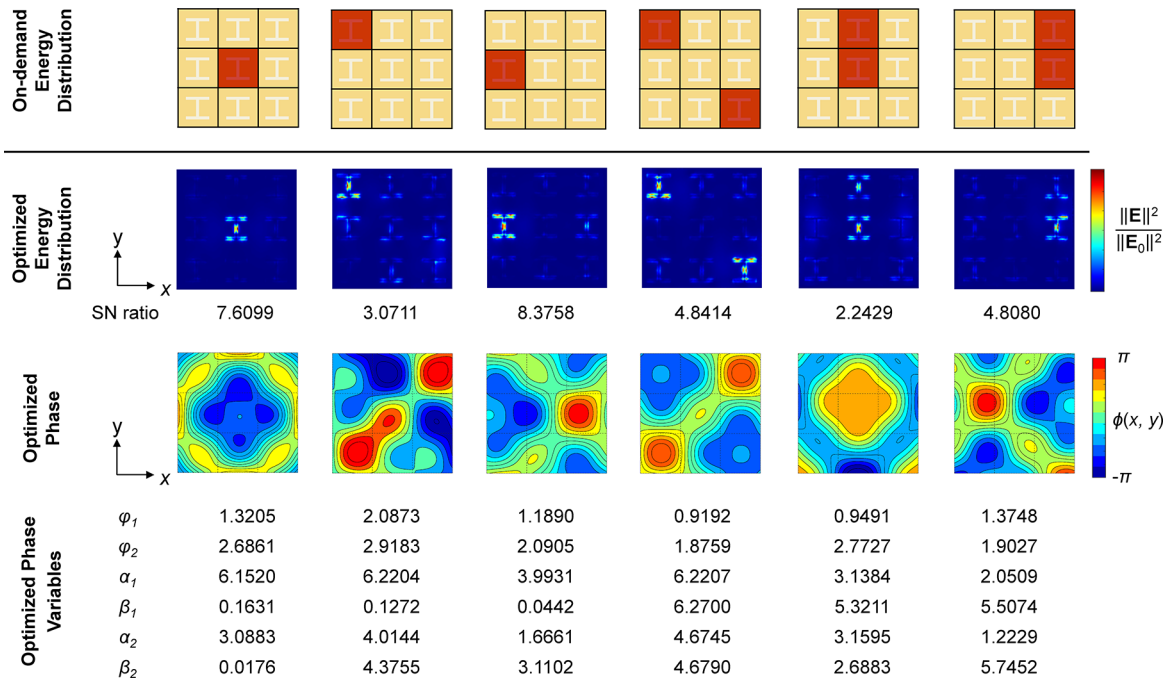

Figure 5. Results of the proposed phase inverse optimization. The first row describes target high-contrast patterns. The red and the yellow cells denote the targeted localization spots and off-target counterparts, respectively. Columns 1−3 address single-hotspot cases, while the other columns do double-hotspot ones. Only independent cases are included considering the symmetry of geometry (I-beam) and polarization (*x*-direction). The second row displays the resulting energy distribution plots of the optimal incident phases. The definition of SN ratio is the same with that in Figure 4. The third row shows the incident profiles optimized with respect to each on-demand pattern. From the results, we conclude that diverse hotspot arrangements can be achieved by our systematic inverse optimization on input phase. The bottom table shows the optimized phase variables that are identified by BO.

is assigned with a large weight to achieve focalization at the center meta-atom, while all the other components are assigned with a smaller weight with the opposite sign to inhibit off-target resonance. The weighted score serves as the figure-of-merit (FoM) of optimization for each target pattern (Figure 3b,c).

OPTIMIZATION METHOD

BO is employed as an efficient global optimizer to perform inverse design on SPM. BO constructs a surrogate model of a highly nonlinear physics-based simulation and sequentially refines it based on new observations.[30,37] The surrogate encodes prior beliefs about a black-box function to be optimized. The prior is iteratively updated by new data. The sequence of observations to be queried is guided by a policy called an acquisition function. It provides the expected utility of unseen samples via balancing exploitation (performance enhancement) and exploration (uncertainty reduction). Derivative-free search of BO renders the optimization process (*i*) less prone to being trapped in local optima (compared to gradient-based approaches), (*ii*) less costly in terms of reaching optima (compared to exhaustive approaches), and (*iii*) flexible in formulating optimization problems (compared to gradient-based approaches). In this study, a Gaussian process[50] is employed as the internal surrogate that captures a nonlinear mapping from phase design variables to plasmonic response and provides prediction uncertainty. Maximization of the expected improvement[29] over the current best is chosen as the infill criteria of BO. We use the *bayesopt* of Statistical and Machine Learning Toolbox in MATLAB[51] for running BO.[30] Section 3 of the Supporting Information provides more formal elaboration on the BO that builds on Gaussian processes and expected improvement.

RESULT

As a proof-of-concept, the I-beam geometry[6] is studied using the proposed optimization method. The incident wave has the incident wavelength λ = 660 nm (f = 454 THz) with *x*-directional polarization. The input phase is modulated by the six design variables of our proposed phase representation in Phase Representation. The periodicity is set as $\Lambda = (2/3)\lambda$ = 440 nm. A unit nanoantenna is made of gold with permittivity ε=-13.682 + 1.3056*i* at f. Periodical tessellation of 30 nm-thick unit cells forms an array that is placed on a $\lambda/2$-thick cuboid of SiO_2 with refractive index n = 1.45. The entire analysis domain is surrounded by perfectly matched layers to suppress boundary reflections. The full-wave analysis is conducted by RF Module of COMSOL Multiphysics.[52] Readers are referred to Figure S3 of Supporting Information for conceptual illustration of the relevant wave analysis.

Figure 4 shows the proposed optimization history of an example where the center focusing pattern is desired. $10D$ = 10 × 6 observations from Latin-hypercube sampling are included as initial space-filling designs,[53] where D is the number of design variables. Once a Gaussian process model in light of the initial database is constructed, sequential search drives the BO procedure. The convergence history of BO (Figure 4) shows an increasing trend of the FoM as the optimization proceeds. The snapshots of the energy distribution plots indicate that output field distributions evolve toward the target pattern as intended.

In addition to the center focalization scenario, we further validate our phase inverse optimization via realizing diverse

https://doi.org/10.1021/acsphotonics.1c01043
ACS Photonics 2022, 9, 351−359

localization patterns. Such patterns are pursued in this study since they can advance SPM-based dynamic localization control (both high-contrast response and pattern diversity). The desired patterns can hardly be achieved through trial-and-error or greedy search in the literature. The core distinction of our approach is that it can systematically identify a required incident phase for any specified target and can address multihotspot patterns as well. Figure 5 shows the optimized phase profile and the resulting on-demand localization over the metasurface array. The optimized energy distributions include a hotspot whose maximum energy intensity is 3 orders of magnitude stronger than the intensity of incident wave. Note that off-target localization is significantly suppressed, contrary to the results from existing works on SPM. This is because the proposed FoM used for BO implicitly takes such unwanted localization into account. In a similar fashion, other on-demand patterns can be easily produced by adjusting **W**. In addition to three single-hotspot patterns, we also report three double-hotspots (Figure 5). All the optimization results reported herein were obtained by running BO several times for each target, which takes into account the stochasticity of the global optimization method. Based on the results, we assert that the BO-based phase optimization enabled advanced SPM-driven dynamic light control as intended. The diverse patterns can quickly switch to one another (*i*) with the help of SLMs whose shift rate is about 200 Hz (comparable to that of piezoelectric control) and (*ii*) without any mechanical adjustment or impact on samples.

CONCLUSION

In summary, we developed a novel optimization procedure on SPM for advanced dynamic localization on plasmonic metasurfaces. Regarding incident phase, we proposed the global harmonic superposition that offers smooth and flexible phase profiles with the compact representation. To expedite optimization, the high-dimensional output field was transformed into a response matrix that encodes high-*D* localization information with reduced dimensionality and much better tractability. We employed BO to efficiently optimize phase of an illumination source given a diverse set of hotspot arrangements. The target patterns were realized over the I-beam metasurface as a proof-of-concept, which is difficult to achieve without systematic search. We believe that the digital addressability is crucial for disseminating practical applications of plasmonic metasurfaces including, but not limited to, optical detection.

We point out two directions of future work that can further advance the SPM-based dynamic control. First, concurrent design that involves both phase design and meta-atom geometry design can be considered. By enlarging the design space, the concurrent design could (*i*) further enhance both response contrast and pattern diversity and (*ii*) build a comprehensive model that encompasses a variety of meta-atom baselines reported in the community.[6,38−44] Second, different forms of phase representations can be investigated. While the proposed phase representation works well for our case study, there may exist other representations that outperform ours with better response contrast or pattern diversity. It is our interest to employ deep learning based generative models[54−58] to enlarge design freedom of phase modulation and to accelerate the relevant forward wave analysis and inverse design.

ASSOCIATED CONTENT

Supporting Information

The Supporting Information is available free of charge at https://pubs.acs.org/doi/10.1021/acsphotonics.1c01043.

(*i*) Far-field optics and influence of diffraction, (*ii*) elaboration on the choice of the proposed harmonic phase representation, (*iii*) basic formulations of Bayesian optimization, and (*iv*) a schematic of wave analysis (PDF)

AUTHOR INFORMATION

Corresponding Author

Wei Chen − *Department of Mechanical Engineering, Northwestern University, Evanston, Illinois 60208, United States;* orcid.org/0000-0002-4653-7124; Email: weichen@northwestern.edu

Authors

Doksoo Lee − *Department of Mechanical Engineering, Northwestern University, Evanston, Illinois 60208, United States;* orcid.org/0000-0002-4597-6643

Shizhou Jiang − *Department of Mechanical Engineering, Northwestern University, Evanston, Illinois 60208, United States*

Oluwaseyi Balogun − *Department of Mechanical Engineering, Northwestern University, Evanston, Illinois 60208, United States;* orcid.org/0000-0002-4159-471X

Complete contact information is available at: https://pubs.acs.org/10.1021/acsphotonics.1c01043

Author Contributions

†These authors contributed equally to this work.

Funding

W.C. acknowledges funding support from the National Science Foundation (NSF) through the CSSI Program (Award #OAC 1835782). O.B. acknowledges support from the NSF through the ECCS program (Award #1611356).

Notes

The authors declare no competing financial interest.

REFERENCES

(1) Chen, H. T.; Taylor, A. J.; Yu, N. A Review of Metasurfaces: Physics and Applications. *Rep. Prog. Phys.* **2016**, *79* (7), 076401.

(2) Bukhari, S. S.; Vardaxoglou, J.; Whittow, W. A Metasurfaces Review: Definitions and Applications. *Appl. Sci.* **2019**, *9* (13), 2727.

(3) Hail, C. U.; Michel, A. K. U.; Poulikakos, D.; Eghlidi, H. Optical Metasurfaces: Evolving from Passive to Adaptive. *Adv. Opt. Mater.* **2019**, *7* (14), 1801786.

(4) Meinzer, N.; Barnes, W. L.; Hooper, I. R. Plasmonic Meta-Atoms and Metasurfaces. *Nat. Photonics* **2014**, *8* (12), 889−898.

(5) Yao, Y.; Shankar, R.; Kats, M. A.; Song, Y.; Kong, J.; Loncar, M.; Capasso, F. Electrically Tunable Metasurface Perfect Absorbers for Ultrathin Mid-Infrared Optical Modulators. *Nano Lett.* **2014**, *14* (11), 6526−6532.

(6) Larouche, S.; Tsai, Y. J.; Tyler, T.; Jokerst, N. M.; Smith, D. R. Infrared Metamaterial Phase Holograms. *Nat. Mater.* **2012**, *11* (5), 450−454.

(7) Arbabi, A.; Horie, Y.; Bagheri, M.; Faraon, A. Dielectric Metasurfaces for Complete Control of Phase and Polarization with Subwavelength Spatial Resolution and High Transmission. *Nat. Nanotechnol.* **2015**, *10* (11), 937−943.

(8) Zhang, K.; Yuan, Y.; Ding, X.; Li, H.; Ratni, B.; Wu, Q.; Liu, J.; Burokur, S. N.; Tan, J. Polarization-Engineered Noninterleaved

Metasurface for Integer and Fractional Orbital Angular Momentum Multiplexing. *Laser Photonics Rev.* **2021**, *15* (1), 2000351.
(9) Yuan, Y.; Zhang, K.; Ratni, B.; Song, Q.; Ding, X.; Wu, Q.; Burokur, S. N.; Genevet, P. Independent Phase Modulation for Quadruplex Polarization Channels Enabled by Chirality-Assisted Geometric-Phase Metasurfaces. *Nat. Commun.* **2020**, *11* (1), 1−9.
(10) Malkiel, I.; Mrejen, M.; Nagler, A.; Arieli, U.; Wolf, L.; Suchowski, H. Plasmonic Nanostructure Design and Characterization via Deep Learning. *Light Sci. Appl.* **2018**, *7* (1), 60.
(11) Cahill, D. G. Analysis of Heat Flow in Layered Structures for Time-Domain Thermoreflectance. *Rev. Sci. Instrum.* **2004**, *75* (12), 5119−5122.
(12) Schmidt, A. J.; Cheaito, R.; Chiesa, M. A Frequency-Domain Thermoreflectance Method for the Characterization of Thermal Properties. *Rev. Sci. Instrum.* **2009**, *80* (9), 094901.
(13) Zhang, X.; Sun, D.; Li, Y.; Lee, G. H.; Cui, X.; Chenet, D.; You, Y.; Heinz, T. F.; Hone, J. C. Measurement of Lateral and Interfacial Thermal Conductivity of Single- and Bilayer MoS2 and MoSe2 Using Refined Optothermal Raman Technique. *ACS Appl. Mater. Interfaces* **2015**, *7* (46), 25923−25929.
(14) Betzig, E.; Chichester, R. J. Single Molecules Observed by Near-Field Scanning Optical Microscopy. *Science* **1993**, *262* (5138), 1422−1425.
(15) Wiesendanger, R. *Scanning Probe Microscopy and Spectroscopy: Methods and Applications*; Cambridge University Press, 1994.
(16) Daly, B. C.; Kang, K.; Wang, Y.; Cahill, D. G. Picosecond Ultrasonic Measurements of Attenuation of Longitudinal Acoustic Phonons in Silicon. *Phys. Rev. B - Condens. Matter Mater. Phys.* **2009**, *80* (17), 1−5.
(17) Balogun, O. Optically Detecting Acoustic Oscillations at the Nanoscale: Exploring Techniques Suitable for Studying Elastic Wave Propagation. *IEEE Nanotechnol. Mag.* **2019**, *13* (3), 39−54.
(18) Sentenac, A.; Chaumet, P. C. Subdiffraction Light Focusing on a Grating Substrate. *Phys. Rev. Lett.* **2008**, *101* (1), 2−5.
(19) Aeschlimann, M.; Bauer, M.; Bayer, D.; Brixner, T.; García De Abajo, F. J.; Pfeiffer, W.; Rohmer, M.; Spindler, C.; Steeb, F. Adaptive Subwavelength Control of Nano-Optical Fields. *Nature* **2007**, *446* (7133), 301−304.
(20) Singh, A.; Hugall, J. T.; Calbris, G.; Van Hulst, N. F. Far-Field Control of Nanoscale Hotspots by Near-Field Interference. *ACS Photonics* **2020**, *7* (9), 2381−2389.
(21) Buijs, R. D.; Wolterink, T. A. W.; Gerini, G.; Verhagen, E.; Koenderink, A. F. Programming Metasurface Near-Fields for Nano-Optical Sensing. *Adv. Opt. Mater.* **2021**, *9* (15), 2100435.
(22) Jenkins, S. D.; Ruostekoski, J. Theoretical Formalism for Collective Electromagnetic Response of Discrete Metamaterial Systems. *Phys. Rev. B* **2012**, *86* (8), na.
(23) Kao, T. S.; Rogers, E. T. F.; Ou, J. Y.; Zheludev, N. I. Digitally" Addressable Focusing of Light into a Subwavelength Hot Spot. *Nano Lett.* **2012**, *12* (6), 2728−2731.
(24) Ertsgaard, C. T.; McKoskey, R. M.; Rich, I. S.; Lindquist, N. C. Dynamic Placement of Plasmonic Hotspots for Super-Resolution Surface-Enhanced Raman Scattering. *ACS Nano* **2014**, *8* (10), 10941−10946.
(25) Gjonaj, B.; Aulbach, J.; Johnson, P. M.; Mosk, A. P.; Kuipers, L.; Lagendijk, A. Active Spatial Control of Plasmonic Fields. *Nat. Photonics* **2011**, *5* (6), 360−363.
(26) Bendsøe, M. P.; Kikuchi, N. Generating Optimal Topologies in Structural Design Using a Homogenization Method. *Comput. Methods Appl. Mech. Eng.* **1988**, *71* (2), 197−224.
(27) Bendsoe, M. P.; Sigmund, O. *Topology Optimization: Theory, Methods, and Applications*; Springer Science & Business Media, 2013.
(28) Jensen, J. S.; Sigmund, O. Topology Optimization for Nano-Photonics. *Laser Photonics Rev.* **2011**, *5* (2), 308−321.
(29) Jones, D. R.; Schonlau, M.; Welch, W. J. Efficient Global Optimization of Expensive Black-Box Functions. *J. Glob. Optim.* **1998**, *13* (4), 455−492.
(30) Shahriari, B.; Swersky, K.; Wang, Z.; Adams, R. P.; De Freitas, N. Taking the Human out of the Loop: A Review of Bayesian Optimization. *Proc. IEEE* **2016**, *104* (1), 148−175.
(31) Sakurai, A.; Yada, K.; Simomura, T.; Ju, S.; Kashiwagi, M.; Okada, H.; Nagao, T.; Tsuda, K.; Shiomi, J. Ultranarrow-Band Wavelength-Selective Thermal Emission with Aperiodic Multilayered Metamaterials Designed by Bayesian Optimization. *ACS Cent. Sci.* **2019**, *5* (2), 319−326.
(32) Whitley, D. A Genetic Algorithm Tutorial. *Stat. Comput.* **1994**, *4* (2), 65−85.
(33) Weile, D. S.; Michielssen, E. Genetic Algorithm Optimization Applied to Electromagnetics: A Review. *IEEE Trans. Antennas Propag.* **1997**, *45* (3), 343−353.
(34) Eberhart, R. C.; Shi, Y. Particle Swarm Optimization: Developments, Applications and Resources. *Proc. IEEE Conf. Evol. Comput. ICEC* **2001**, *1*, 81−86.
(35) Choudhury, B.; Manickam, S.; Jha, R. M. Particle Swarm Optimization for Multiband Metamaterial Fractal Antenna. *J. Optim.* **2013**, *2013*, 1−8.
(36) Whiting, E. B.; Campbell, S. D.; Kang, L.; Werner, D. H. Meta-Atom Library Generation via an Efficient Multi-Objective Shape Optimization Method. *Opt. Express* **2020**, *28* (16), 24229.
(37) Snoek, J.; Larochelle, H.; Adams, R. P. Practical Bayesian Optimization of Machine Learning Algorithms. *Adv. Neural Inf. Process. Syst.* **2012**, *4*, 2951−2959.
(38) Liu, X.; Tyler, T.; Starr, T.; Starr, A. F.; Jokerst, N. M.; Padilla, W. J. Taming the Blackbody with Infrared Metamaterials as Selective Thermal Emitters. *Phys. Rev. Lett.* **2011**, *107* (4), 045901.
(39) Blanchard, R.; Aoust, G.; Genevet, P.; Yu, N.; Kats, M. A.; Gaburro, Z.; Capasso, F. Modeling Nanoscale V-Shaped Antennas for the Design of Optical Phased Arrays. *Phys. Rev. B - Condens. Matter Mater. Phys.* **2012**, *85* (15), 155457.
(40) Choi, M.; Lee, S. H.; Kim, Y.; Kang, S. B.; Shin, J.; Kwak, M. H.; Kang, K. Y.; Lee, Y. H.; Park, N.; Min, B. A Terahertz Metamaterial with Unnaturally High Refractive Index. *Nature* **2011**, *470* (7334), 369−373.
(41) Plum, E.; Zhou, J.; Dong, J.; Fedotov, V. A.; Koschny, T.; Soukoulis, C. M.; Zheludev, N. I. Metamaterial with Negative Index Due to Chirality. *Phys. Rev. B - Condens. Matter Mater. Phys.* **2009**, *79* (3), 035407.
(42) Yang, Y.; Kravchenko, I. I.; Briggs, D. P.; Valentine, J. All-Dielectric Metasurface Analogue of Electromagnetically Induced Transparency. *Nat. Commun.* **2014**, *5* (1), 5753.
(43) Yi, C.; Dongare, P. D.; Su, M. N.; Wang, W.; Chakraborty, D.; Wen, F.; Chang, W. S.; Sader, J. E.; Nordlander, P.; Halas, N. J.; Link, S. Vibrational Coupling in Plasmonic Molecules. *Proc. Natl. Acad. Sci. U. S. A.* **2017**, *114* (44), 11621−11626.
(44) Jenkins, S. D.; Papasimakis, N.; Savo, S.; Zheludev, N. I.; Ruostekoski, J. Strong Interactions and Subradiance in Disordered Metamaterials. *Phys. Rev. B* **2018**, *98* (24), 245136.
(45) Kiarashinejad, Y.; Zandehshahvar, M.; Abdollahramezani, S.; Hemmatyar, O.; Pourabolghasem, R.; Adibi, A. Knowledge Discovery in Nanophotonics Using Geometric Deep Learning. *Adv. Intell. Syst.* **2020**, *2* (2), 1900132.
(46) Vashistha, V.; Vaidya, G.; Hegde, R. S.; Serebryannikov, A. E.; Bonod, N.; Krawczyk, M. All-Dielectric Metasurfaces Based on Cross-Shaped Resonators for Color Pixels with Extended Gamut. *ACS Photonics* **2017**, *4* (5), 1076−1082.
(47) Prodan, E.; Radloff, C.; Halas, N. J.; Nordlander, P. A Hybridization Model for the Plasmon Response of Complex Nanostructures. *Science* **2003**, *302* (5644), 419−422.
(48) Moffitt, J. R.; Chemla, Y. R.; Smith, S. B.; Bustamante, C. Recent Advances in Optical Tweezers. *Annu. Rev. Biochem.* **2008**, *77*, 205−228.
(49) Huang, L.; Chen, X.; Mühlenbernd, H.; Zhang, H.; Chen, S.; Bai, B.; Tan, Q.; Jin, G.; Cheah, K. W.; Qiu, C. W.; Li, J.; Zentgraf, T.; Zhang, S. Three-Dimensional Optical Holography Using a Plasmonic Metasurface. *Nat. Commun.* **2013**, *4* (May), 1−8.

https://doi.org/10.1021/acsphotonics.1c01043
ACS Photonics 2022, 9, 351−359

(50) Rasmussen, C. E. *Gaussian Processes in Machine Learning*; Springer, 2003.
(51) MATLAB, v. R2021a, https://www.mathworks.com (accessed 2021−12−12).
(52) COMSOL Multiphysics, v. 5.3, https://www.comsol.com (accessed 2021−12−12).
(53) Loeppky, J. L.; Sacks, J.; Welch, W. J. Choosing the Sample Size of a Computer Experiment: A Practical Guide. *Technometrics* **2009**, *51* (4), 366−376.
(54) Liu, Z.; Zhu, D.; Rodrigues, S. P.; Lee, K. T.; Cai, W. Generative Model for the Inverse Design of Metasurfaces. *Nano Lett.* **2018**, *18* (10), 6570−6576.
(55) Ma, W.; Cheng, F.; Xu, Y.; Wen, Q.; Liu, Y. Probabilistic Representation and Inverse Design of Metamaterials Based on a Deep Generative Model with Semi-Supervised Learning Strategy. *Adv. Mater.* **2019**, *31* (35), 1901111.
(56) Molesky, S.; Lin, Z.; Piggott, A. Y.; Jin, W.; Vuckovic, J.; Rodriguez, A. W. Inverse Design in Nanophotonics. *Nat. Photonics* **2018**, *12* (11), 659−670.
(57) So, S.; Rho, J. Designing Nanophotonic Structures Using Conditional Deep Convolutional Generative Adversarial Networks. *Nanophotonics* **2019**, *8* (7), 1255−1261.
(58) Wiecha, P. R.; Muskens, O. L. Deep Learning Meets Nanophotonics: A Generalized Accurate Predictor for near Fields and Far Fields of Arbitrary 3D Nanostructures. *Nano Lett.* **2020**, *20* (1), 329−338.

https://doi.org/10.1021/acsphotonics.1c01043
ACS Photonics 2022, 9, 351−359